New acoustic approximation for the transversely isotropic media with a vertical symmetry axis

Shibo Xu[1], Alexey Stovas[2], Tariq Alkhalifah[3] and Hitoshi Mikada[1]

[1]Department of Civil and Earth Resources Engineering, Kyoto University, C1-1-111 Kyotodaigaku-Katsura, Nishikyo-ku, Kyoto, Japan

[2]Department of Geoscience and Petroleum, Norwegian University of Science and Technology, S.P. Andersens veg 15a, NO-7491 Trondheim, Norway

[3]Astronomy and Geophysical Research Institute, King Abdullah University of Science and Technology, Thuwal, Saudi Arabia.

Running head: New acoustic approximation

Keywords: acoustic, VTI model, Seismic modeling

Abstract

Seismic data processing in the elastic anisotropic model is complicated due to multi-parameters-dependency. Approximations to the P-wave kinematics are necessary for practical purposes. The acoustic approximation for P-waves in a transversely isotropic medium with a vertical symmetry axis (VTI) simplifies the description of wave propagation in elastic media, and as a result, it is widely adopted in seismic data processing and analysis. However, finite-difference implementations of that approximation are plagued with shear-wave artifacts. Specifically, the resulting wavefield also includes artificial diamond-shaped S-waves resulting in a redundant signal for many applications that require pure P-wave data. To derive a totally S-wave free acoustic approximation, we propose a new acoustic approximation for pure P-waves that is totally free of S-wave artifacts in the homogenous VTI model. To keep the S-wave velocity equal to zero, we formulate the vertical S-wave velocity to be a function of the model parameters, rather than simply setting it to zero. Then, the corresponding P-wave phase and group velocities for the new acoustic approximation are derived. For this new acoustic approximation, the kinematics is described by a new eikonal equation for pure P-wave propagation, which defines the new vertical slowness for the P-waves. The corresponding perturbation-based approximation for our new eikonal equation is used to compare the new equation with the original acoustic eikonal. The accuracy of our new P-wave acoustic approximation is tested on numerical examples for homogeneous and multilayered VTI models. We find that the accuracy of our new acoustic approximation is as good as the original one for the phase velocity, group velocity and the kinematic parameters like the vertical slowness, traveltime and the relative geometrical spreading. Therefore, the S-wave-free acoustic approximation could be further applied in seismic processing that requires pure P-wave data.

Introduction

Compared to isotropic media, the velocity in anisotropic media changes with propagation direction and such velocity variation is controlled by more than one parameter. Due to the multi-parameters dependence, the equations describing the phase and group velocities in anisotropic media are quite complicated. The complexity in the elastic anisotropic model results in a heavy computational cost. For simplification purposes, some approximations like the weak anisotropy approximation, elliptical approximation (Dellinger and Muir, 1988) and small dip angle approximation (Cohen, 1996) were proposed to reduce the computational cost. However, the accuracy of these methods is limited. Alkhalifah (1998) proposed the acoustic approximation for P-waves by setting the value of the vertical S-wave velocity to zero. This modification contributed a lot in time-related processing like moveout correction, dip moveout and time migration that are almost vertical S-wave independent by properly selecting the model parameterization. The influence from setting the value of vertical S-wave to be zero is nearly negligible while, as a consequence, the corresponding expression describing the elastic model is simplified greatly. Subsequently, an acoustic wave equation for a transversely isotropic medium with a vertical symmetry axis (VTI) is proposed by Alkhalifah (2000).

This acoustic representation provides a reasonably accurate approximation to P-wave propagation in elastic media by accurately describing the P-wave kinematics and boosting the efficiency of imaging and other seismic processing applications, and as a result, it is widely adopted in both industry and academia. Using the acoustic dispersion relation, additional variations of acoustic anisotropic wave equation were proposed for VTI (Zhou et al., 2006) and transversely isotropic media with tilted axis (TTI) of symmetry (Fletcher et al., 2009). The acoustic assumption could be applied in reverse time migration (RTM) in TI media (Alkhalifah, 2000) resulting a large reduction in computational cost. The acoustic concept is

commonly adopted by our Geophysical community and widely applied for almost all seismic data process methods like seismic modeling (Finkelstein and Kastner, 2007; Liu and Sen, 2010), underground imaging (Alkhalifah and Fomel, 2011; Li et al., 2016; Xu et al., 2016), full waveform inversion (FWI) (Gholami et al., 2013; Alkhalifah and Plessix, 2014) and traveltime tomography (Wang and Tsvankin, 2013, Li et al., 2017). However, mitigating the accompanying S-wave artifacts often requires additional processing or limiting assumptions. This acoustic assumption ($v_{s0} = 0$) does not mean that the S-wave propagation is fully removed. Using this acoustic approximation, and considered as an unwanted artifact, a diamond-shaped S-wave appears in the wavefield (Grechka et al., 2004; Jin and Stovas, 2018). This S-wave artifact results in a redundant signal for many applications that require pure P-wave data. The kinematics of this acoustic S-wave is defined and analyzed by Jin and Stovas (2018).

In order to remove these artifacts, Alkhalifah (2000) suggested putting the sources and receivers in a purely isotropic or elliptical anisotropic medium. Fomel et al. (2013) proposed to adopt a mixed-domain extrapolation for P-waves to avoid the generation of these S-waves. In order to eliminate these unwanted S-wave energy totally, many methods for the pure P-wave propagation have been proposed. Du et al. (2010) used the optimized separable approximation, which separates P and S-waves. Also, methods like the Rapid Expansion (RE) (Pestana and Stoffa, 2010), the Fourier Finite Difference (FFD) (Song and Fomel, 2011), the Low Rank (LR) approximation (Song and Alkhalifah, 2013 and Alkhalifah, 2013) and the P-wave propagator separation (Cheng and Kang, 2014) method could also achieve the purpose of approximating the pure P-wave in VTI model. Using the artifact-free isotropic and elliptically anisotropic modeling in an effective anisotropic model (Ibanez-Jacome et. al., 2013; Waheed and Alkhalifah, 2015) is another possible way to remove S-waves. Notice that some attempts above like the LR approximation, artifact-free isotropic model and the

elliptically anisotropic modeling suffer from low accuracy in describing the pure P-wave propagation due to the approximation used in the phase velocities or the dispersion relations. In this paper, we propose a new acoustic approximation for the VTI model. Compared with the original acoustic approximation (Alkhalifah, 1998), our method is defined for pure P-waves where S-wave artifacts are fully eliminated, which can provide an alternative wave equation needed in pure P-wave processing. The corresponding P-wave phase and group velocities for the new approximation are derived as well as a new eikonal equation that describes the pure P-wave traveltimes. A comparison with the original acoustic approximation in the accuracy of the phase velocity, the group velocity and the kinematic parameters like vertical slowness, traveltime and the corresponding relative geometrical spreading are performed using numerical examples. Although our new acoustic approximation is more complex than the standard one (Alkhalifah, 1998), the totally S-wave free character is very useful for the seismic processing methods that require pure P-wave data.

Elastic and acoustic VTI media

The wavefront (phase) velocities for P- and S-waves in elastic VTI media are extracted from the Christoffel equation, and given by Thomsen (1986)

$$v^2(\theta) = \frac{C_{33} + C_{44} + (C_{11} - C_{33})\sin(\theta)^2 \pm F}{2}, \tag{1}$$

with

$$\begin{aligned} F = \Big\{ &(C_{33} - C_{44})^2 + 2\Big[2(C_{13} + C_{44})^2 - (C_{33} - C_{44})(C_{11} + C_{33} - 2C_{44})\Big]\sin(\theta)^2 \\ &+ \Big[(C_{11} + C_{33} - 2C_{44})^2 - 4(C_{13} + C_{44})^2\Big]\sin(\theta)^4 \Big\}^{1/2}, \end{aligned} \tag{2}$$

where C_{ij} are the stiffness coefficients, θ is the phase angle, and the positive sign in equation 1 corresponds to the velocity for P-waves while the negative sign corresponds to the velocity for S-waves. Notice that the S-wave corresponds to the SV shear wave polarized in the

vertical plane. These stiffness coefficients are related to the anisotropy parameters (v_{pn} and η) and Thomsen (1986) parameters (δ and ε) as follows (Alkhalifah, 1998)

$$\begin{aligned} &C_{11}=(1+2\eta)v_{pn}^2,\ C_{33}=v_{p0}^2,\ C_{44}=v_{s0}^2,\ C_{13}=\sqrt{(v_{p0}^2-v_{s0}^2)(v_{pn}^2-v_{s0}^2)}-v_{s0}^2; \\ &C_{11}=(1+2\varepsilon)v_{p0}^2,\ C_{33}=v_{p0}^2,\ C_{44}=v_{s0}^2,\ C_{13}=\sqrt{(v_{p0}^2-v_{s0}^2)\left[(1+2\delta)v_{p0}^2-v_{s0}^2\right]}-v_{s0}^2, \end{aligned} \tag{3}$$

where v_{p0} and v_{s0} are vertical velocities for the P- and S-waves, respectively, v_{pn} is the P-wave normal moveout (NMO) velocity defined as $v_{pn}=v_{p0}\sqrt{1+2\delta}$, and η is the anellipticity parameter defined as $\eta=(\varepsilon-\delta)/(1+2\delta)$ (Alkhalifah, 1998), where δ and ε are the anisotropic parameters defined by Thomsen (1986). By substituting equation 3 into equation 1, the explicit expressions for P and S phase velocities, in terms of the anisotropic parameters (Thomsen, 1986),

$$\begin{aligned} v_p^2(\theta)&=\frac{v_{p0}^2+v_{s0}^2+\left[(1+2\eta)v_{pn}^2-v_{p0}^2\right]\sin(\theta)^2+E}{2}, \\ v_s^2(\theta)&=\frac{v_{p0}^2+v_{s0}^2+\left[(1+2\eta)v_{pn}^2-v_{p0}^2\right]\sin(\theta)^2-E}{2}, \end{aligned} \tag{4}$$

with

$$\begin{aligned} E=\Big\{&\left(v_{p0}^2-v_{s0}^2\right)^2-2\left[v_{p0}^2+(1+2\eta)v_{pn}^2\right]\left(v_{p0}^2-v_{s0}^2\right)\sin(\theta)^2 \\ &+\left[v_{p0}^4+2(1+2\eta)v_{pn}^2v_{p0}^2+(1+2\eta)^2v_{pn}^4-8\eta v_{pn}^2v_{s0}^2\right]\sin(\theta)^4\Big\}^{1/2}. \end{aligned} \tag{5}$$

Due to the often surface acquisition nature of our seismic data, and the more often vertical symmetry axis nature of the Earth, characterizing the model by the NMO velocity v_{pn} and the anellipticity parameter η, the impact of the vertical P-wave (v_{p0}) and S-wave (v_{s0}) on P-wave data is negligible (Alkhalifah, 1998). By setting the value of the vertical S-wave to be zero ($v_{s0}\to 0$), the expression for the P-wave velocity is much simpler and easier:

$$v_p^2(\theta) = \frac{1}{2}\left\{v_{p0}^2 + \left[(1+2\eta)v_{pn}^2 - v_{p0}^2\right]\sin(\theta)^2 + \sqrt{v_{p0}^4 - 2\left[v_{p0}^2 + (1+2\eta)v_{pn}^2\right]v_{p0}^2\sin(\theta)^2 + \left[v_{p0}^4 + 2(1+2\eta)v_{pn}^2v_{p0}^2 + (1+2\eta)^2 v_{pn}^4\right]\sin(\theta)^4}\right\}. \quad (6)$$

The corresponding ray (group) velocity can be computed using the derivatives of the phase velocity as given by Berryman (1979)

$$V_p^2(\theta) = v_p^2(\theta) + \left(\frac{\partial v_p(\theta)}{\partial\theta}\right)^2, \quad (7)$$

The vertical and horizontal components of the group velocity (Tsvankin, 2012) are computed as

$$\begin{aligned} V_p^2(\phi = 90^\circ) &= v_p^2(\theta)\cos(\theta) - \frac{\partial v_p(\theta)}{\partial\theta}\sin(\theta), \\ V_p^2(\phi = 0^\circ) &= v_p^2(\theta)\sin(\theta) + \frac{\partial v_p(\theta)}{\partial\theta}\cos(\theta), \end{aligned} \quad (8)$$

where ϕ is the group angle. The group angle can be represented as a function of the phase angle

$$\tan(\theta) = \frac{\tan(\theta) + \frac{1}{v_p}\frac{\partial v_p}{\partial\theta}}{1 - \frac{\tan(\theta)}{v_p}\frac{\partial v_p}{\partial\theta}}. \quad (9)$$

Two VTI models are introduced for our computation where the model parameters are defined in Table 1. We can see that the anisotropy in the VTI 2 model is very strong. We plot the phase and group velocities of the elastic P and S-waves from equation 4 for the two defined VTI models in Figure 1. One can see that the P-wave phase and group velocities are very similar. However, the abnormal curve (concave shape) is obtained for S-waves in VTI model 2 for the phase velocity which results in a triplication in the group velocity plot.

The relative errors in the P-wave phase and group velocities using the original acoustic approximation (Alkhalifah, 1998) are shown in Figure 2, top and bottom, respectively. We

can see that the errors from using the acoustic approximation are slightly larger for VTI model 2 while the value in the error is very small. Our new acoustic approximation could be applied to provide a reasonably accurate phase and group velocities.

The acoustic approximation simplifies the P-wave expression a lot taking into consideration that the errors are almost negligible. However, setting vertical S-wave velocity to zero does not mean that the S-waves are totally eliminated. The S-wave artifacts resulting from the acoustic P-wave equation still remains and is shown in the snapshot of the wavefield in Figure 3 (Jin and Stovas, 2018). This artifact has a large imprint in practice, which may cause degradation of the seismic imaging and FWI results (Gholami et al., 2013).

The new acoustic approximation in VTI media

In order to obtain a pure P-wave acoustic approximation in VTI media, instead of setting the vertical S-wave to zero ($v_{s0} = 0$) where the phase velocity of the shear wave is zero for the given specific phase angle only, and non-zero for all other directions, including the axial direction, we set the function of S-wave phase velocity shown in equation 4 to zero ($v_s(\theta) = 0$). We then compute the resulting vertical S-wave velocity ($v_{s0}(\theta)$) as a function of the phase angle. The explicit form for P and S-wave phase velocities are given in equation 4. This is the exact form for P and S-wave phase velocities and no approximation is involved. The standard acoustic approximation (Alkhalifah, 1998) is obtained by setting the vertical S velocity to be zero ($v_{s0} \to 0$) in $v_p(\theta)$.

The expression for the vertical S-wave $v_{s0}(\theta)$ could be computed from equation 4 as follows:

$$v_{s0}^2(\theta) = \frac{\left(v_s^2(\theta) - v_{p0}^2\right)v_s^2(\theta) + \left[2\eta v_{pn}^2 + \left(v_{p0}^2 - v_s^2(\theta)\right) + \left(v_{p0}^2 - v_{pn}^2\right)v_s^2(\theta)\right]\sin(\theta)^2 - 2\eta v_{p0}^2 v_{pn}^2 \sin(\theta)^4}{v_s^2(\theta) - v_{p0}^2 + \left(v_{p0}^2 - v_{pn}^2\right)\sin(\theta)^2 - 2\eta v_{pn}^2 \sin(\theta)^4}. \quad (10)$$

In order to eliminate the S-waves, we set the S-waves function to zero ($v_s(\theta) = 0$). The vertical S-wave velocity is no longer constant, but a function of model parameters ($v_{s0}(\theta)$) given by

$$v_{s0}^2(\theta) = -\frac{2\eta v_{p0}^2 v_{pn}^2 \sin(\theta)^2 \cos(\theta)^2}{v_{p0}^2 + (v_{pn}^2 - v_{p0}^2)\sin(\theta)^2 + 2\eta v_{pn}^2 \sin(\theta)^4}. \tag{11}$$

Notice that here the vertical S-wave velocity in equation 11 becomes a function ($v_{s0}(\theta)$) instead of a model parameter to keep the value of the S-wave velocity ($v_s(\theta)$) equal to zero for all phase angles.

By substituting the form of the vertical S-wave velocity shown in equation 11 into the expression for the P-wave velocity in equation 4, we obtain the pure acoustic P-wave phase velocity function

$$v_p^2(\theta) = \frac{v_{p0}^4 + \sin(\theta)^2 \left[v_{p0}^2 - v_{pn}^2 \left(1 + 2\eta \sin(\theta)^2\right)\right]\left[v_{p0}^2 - v_{pn}^2 \left(1 + 2\eta\right)\sin(\theta)^2 - 2v_{p0}^2 \right]}{v_{p0}^2 + (v_{pn}^2 - v_{p0}^2)\sin(\theta)^2 + 2\eta v_{pn}^2 \sin(\theta)^4}. \tag{12}$$

Note that since the horizontally polarized shear wave is decoupled from both compressional waves and vertically polarized shear waves, the phase velocities of P and S-waves are defined by a quadratic equation, whose coefficients depend on the phase angle θ. The smaller root of this quadratic equation is assumed to be zero, which means that the constant term of the quadratic trinomial is zero. The vanishing constant term of the quadratic equation is actually the condition for our suggested approximation. The remaining (compressional wave) root is delivered by a linear equation. That is why our equation 12 is rational, no square root operator is needed to find $v_p^2(\theta)$.

We plot the function for the vertical S-wave velocity in equation 11 for the two defined VTI models in Figure 4. We can see from the polar plot that in order to keep the S-wave velocity equal to zero at all angles, the value of the vertical S-wave velocity should depend on the propagation angle. It is zero along the vertical and horizontal directions, while for other

angles the value of the vertical S-wave is non-zero and depends on the model parameters and the current phase angle θ. By setting the S-wave velocity shown in equation 4 to zero, our new acoustic approximation for P-wave velocities shown in equation 12 will not include S-waves. We plot the group velocity for VTI model 1 for the elastic case, as well as, for the original acoustic approximation (Alkhalifah, 1998) and for our new acoustic approximation in Figure 5 a, b and c, respectively. Notice that the expression for the S-wave artifact from the original acoustic approximation could be found in Song and Stovas (2018). One can see from the plots that for the original acoustic approximation, the S-wave artifacts still remain, which could be seen from the snapshot in Figure 3. On the contrary, for our new acoustic approximation, only P-waves are present and the S-wave artifact is totally removed.

In order to test the difference between the two acoustic approximations, we plot the relative error in phase and group velocities for the two introduced VTI models in Figure 6. Compared to the results computed in VTI model 1, the error in VTI model 2 is larger in both phase and group velocity regardless of which of the acoustic approximations are used. For the error in phase and group velocities, the original acoustic approximation (Alkhalifah, 1998) is more accurate in VTI model 1 while less accurate in VTI model 2.

Kinematics of the new acoustic approximation in VTI media

The vertical slowness for elastic VTI media is obtained by solving the cubic equation that results from setting the determinant of the Christoffel matrix to zero as shown in Appendix A. Then the vertical slowness for acoustic VTI media is obtained by setting the vertical S-wave to be zero as shown in Appendix A.

On the other hand, the vertical slowness for P-waves using our new acoustic approximation is derived from the following eikonal form extracted from the phase velocity expression,

$$
\begin{aligned}
v_p^2(\theta) &= \frac{1}{p_x^2 + p_z^2}, \\
\sin^2(\theta) &= \frac{p_x^2}{p_x^2 + p_z^2}, \cos^2(\theta) = \frac{p_z^2}{p_x^2 + p_z^2},
\end{aligned}
\tag{13}
$$

where p_x and p_y are the projections of the horizontal and vertical slowness vector with $p_x = \sin(\theta)/v(\theta)$ and $p_z = \cos(\theta)/v(\theta)$. The relationship between the two Cartesian slowness components could be obtained by replacing $\sin^2(\theta)$ and v_p^2 in equation 13.

After some algebraic manipulation, the vertical slowness is computed by solving the following cubic equation (shown in Appendix B)

$$
p_z^6 + Bp_z^4 + Cp_z^2 + D = 0, \tag{14}
$$

where the coefficients B, C and D are given by

$$
\begin{aligned}
B &= \frac{p_x^2\left(v_{p0}^2 + 2v_{pn}^2\right) - 1}{v_{p0}^2}, \\
C &= \frac{p_x^2\left(\left(2(1+\eta)\, p_x^2 v_{pn}^2 - 1\right)\left(v_{p0}^2 + v_{pn}^2\right)\right)}{v_{p0}^4}, \\
D &= \frac{p_x^4 v_{pn}^2 (1+2\eta)\left((1+2\eta)\, p_x^2 v_{pn}^2 - 1\right)}{v_{p0}^4}.
\end{aligned}
\tag{15}
$$

The solution for the vertical slowness squared is given by

$$
p_z^2 = \frac{1}{6}\left[-2B + \frac{2\times 2^{1/3} f_1}{\left(f_2 + f_3\right)^{1/3}} + 2^{2/3}\left(f_2 + f_3\right)^{1/3}\right], \tag{16}
$$

with

$$
\begin{aligned}
f_1 &= B^2 - 3C, \\
f_2 &= -2B^3 + 9BC - 27D, \\
f_3 &= 3\sqrt{3}\sqrt{-B^2C^2 + 4C^3 + 4B^3D - 18BCD + 27D^2}.
\end{aligned}
\tag{17}
$$

The discriminant of the cubic equation is used to determine the number of real and complex roots as shown in equation B-4. The stability analysis is applied by properly selecting the anisotropic parameters to keep the discriminant of the cubic equation to be negative. We

select the values of the model parameters as $v_{p0}=3\text{km/s}$, $v_{s0}=1\text{km/s}$ and $z_0=1\text{km}$, and plot the discriminant versus two anisotropic parameters δ and ε as shown in Figure 7. We can tell that for stability purposes, the range of δ and ε needs to be selected carefully to keep the discriminant of the cubic equation negative.

By differentiating equation 14 over p_x, we obtain

$$2p_z\frac{dp_z}{dp_x}\left(3p_z^4+2Bp_z^2+C\right)+\frac{dB}{dp_x}p_z^4+\frac{dC}{dp_x}p_z^2+\frac{dD}{dp_x}=0 \tag{18}$$

From this equation, we have

$$\frac{dp_z}{dp_x}=-\frac{\frac{dB}{dp_x}p_z^4+\frac{dC}{dp_x}p_z^2+\frac{dD}{dp_x}}{2p_z\left(3p_z^4+2Bp_z^2+C\right)} \tag{19}$$

where

$$\begin{aligned}
\frac{dB}{dp_x}&=\frac{2p_x\left(v_{p0}^2+2v_{pn}^2\right)}{v_{p0}^2},\\
\frac{dC}{dp_x}&=-\frac{2p_x\left(v_{p0}^2+v_{pn}^2\right)\left(1-4\left(1+\eta\right)p_x{}^2v_{pn}^2\right)}{v_{p0}^4},\\
\frac{dD}{dp_x}&=-\frac{2p_x^3v_{pn}^3\left(1+2\eta\right)\left(2-3\left(1+2\eta\right)p_x{}^2v_{pn}^2\right)}{v_{p0}^4}.
\end{aligned} \tag{20}$$

The phase velocity and angle can be computed from the vertical and horizontal slowness using

$$\begin{aligned}
\tan(\theta)&=\frac{p_x}{p_z},\\
v_p^2&=\frac{1}{p_x^2+p_z^2}.
\end{aligned} \tag{21}$$

The group velocity and angle can also be computed from the slowness and its derivative. Therefore, the group angle and velocity are given by

$$\tan(\phi) = -\frac{\partial p_z}{\partial p_x} = \frac{\frac{dB}{dp_x} p_z^4 + \frac{dC}{dp_x} p_z^2 + \frac{dD}{dp_x}}{2p_z\left(3p_z^4 + 2Bp_z^2 + C\right)},$$
$$\frac{1}{V_p} = p_z - p_x \frac{\partial p_z}{\partial p_x} = p_z + p_x \frac{\frac{dB}{dp_x} p_z^4 + \frac{dC}{dp_x} p_z^2 + \frac{dD}{dp_x}}{2p_z\left(3p_z^4 + 2Bp_z^2 + C\right)}. \quad (22)$$

Note that different from the "standard" acoustic case, there is no S-wave component at all but two more complex conjugate solutions, which is not used. The eikonal equation (a Partial Differential Equation (PDE)) describes a level set object representing the traveltime of waves in the earth's subsurface. The acoustic eikonal equation derived by Alkhalifah (2000) is given by

$$v_{pn}^2\left(1+2\eta\right)\left(\frac{\partial \tau}{\partial x}\right)^2 + v_{p0}^2\left(\frac{\partial \tau}{\partial z}\right)^2 - 2\eta v_{pn}^2 v_{p0}^2\left(\frac{\partial \tau}{\partial x}\right)^2\left(\frac{\partial \tau}{\partial z}\right)^2 = 1. \quad (23)$$

This original acoustic approximation results in a fourth-order PDE. The perturbation-based approximation up to the second-order in the anellipticity parameter η for the eikonal in equation 23 is given by Alkhalifah (2011)

$$\tau_{old} = \sqrt{t_0^2 + t_n^2} - \frac{t_n^4}{\left(t_0^2 + t_n^2\right)^{3/2}}\eta + \frac{3\left(4t_0^2 t_n^6 + t_n^8\right)}{2\left(t_0^2 + t_n^2\right)^{7/2}}\eta^2, \quad (24)$$

where $t_0 = z_0 / v_{p0}$ and $t_n = x / v_{pn}$.

Our new derived acoustic eikonal equation is given by the form

$$\left[\left(\frac{\partial \tau}{\partial x}\right)^2 + \left(\frac{\partial \tau}{\partial z}\right)^2\right]\left[v_{Pn}^2\left(\frac{\partial \tau}{\partial x}\right)^2 + v_{P0}^2\left(\frac{\partial \tau}{\partial z}\right)^2 - 1\right]\left[v_{PN}^2\left(\frac{\partial \tau}{\partial x}\right)^2 + v_{P0}^2\left(\frac{\partial \tau}{\partial z}\right)^2\right] +$$
$$2\eta v_{Pn}^2\left(\frac{\partial \tau}{\partial x}\right)^4\left\{v_{PN}^2\left(\frac{\partial \tau}{\partial x}\right)^2 + v_{P0}^2\left(\frac{\partial \tau}{\partial z}\right)^2 - 1 + v_{PN}^2\left[\left(\frac{\partial \tau}{\partial x}\right)^2 + \left(\frac{\partial \tau}{\partial z}\right)^2\right]\right\} + 4\eta^2 v_{Pn}^4\left(\frac{\partial \tau}{\partial x}\right)^6 = 0 \quad (25)$$

Different from the eikonal equation 19, our new acoustic eikonal equation above results in a sixth-order PDE with one real and two complex conjugate solutions, where the real solution could be used for the pure acoustic wave propagation for seismic data processing.

The perturbation-based approximation for the original eikonal equation 25 is given by Xu et al., (2017)

$$\tau_{new} = \sqrt{t_0^2 + t_n^2} - \frac{t_n^4}{\left(t_0^2 + t_n^2\right)^{3/2}}\eta + \frac{t_n^6\left[3t_n^4 v_{p0}^2 - 4t_0^4\left(v_{p0}^2 - 4v_{pn}^2\right)\right] + 3t_0^2 t_n^2\left(4v_{p0}^2 + v_{pn}^2\right)}{2\left(t_0^2 + t_n^2\right)^{7/2}\left(t_0^2 v_{pn}^2 + t_n^2 v_{p0}^2\right)}\eta^2. \tag{26}$$

where the perturbed value is the anellipticity η as in equation 24. We can see that the difference in the perturbation coefficients comes out from the second-order coefficient.

The P-wave traveltimes and offsets are computed from the derivation of the corresponding P-wave vertical slowness (Tsvankin, 2012; Xu and Stovas, 2017)

$$\begin{aligned} x &= -z\frac{\partial p_z}{\partial p_x}, \\ t &= zp_z + xp_x, \end{aligned} \tag{27}$$

where z is the depth of the reflector.

The Taylor series expansion in terms of offset for the traveltime square using the original and new acoustic approximations up to the sixth-order are

$$\begin{aligned} t_{old}^2 &= \frac{z_0^2}{v_{p0}^2} - \frac{1}{v_{pn}^2}x^2 + \frac{(1+6\eta)v_{p0}^2}{v_{pn}^4 z_0^2}x^4 - \frac{\left[\left(1+18\eta+60\eta^2\right)v_{p0}^2 - V_{pn}^2 z_0^2\right]v_{p0}^2}{v_{pn}^8 z_0^4}x^6, \\ t_{new}^2 &= \frac{z_0^2}{v_{p0}^2} - \frac{1}{v_{pn}^2}x^2 + \frac{(1+6\eta)V_{p0}^2}{v_{pn}^4 z_0^2}x^4 + \frac{20\eta^2 v_{p0}^6 - (1+8\eta)(1+10\eta)v_{p0}^4 v_{pn}^2 + v_{p0}^2 v_{pn}^4 z_0^2}{v_{pn}^8 z_0^4}x^6. \end{aligned} \tag{28}$$

The difference in the series coefficients using two acoustic approximations starts to appear at the sixth-order term. For VTI model 1, the sixth-order moveout coefficients are -0.13736 and -0.13953 for old and new acoustic approximations, respectively. For VTI model 2, the sixth-order moveout coefficients for old and new acoustic approximations are: 0.0391 and 0.0374, respectively.

The relative geometrical spreading of P-waves can also be obtained from the derivatives of the vertical slowness given by (Stovas and Ursin, 2009; Xu and Stovas, 2018)

$$\mathcal{L}_N = \left(\frac{x}{p_x} \frac{\partial x}{\partial p_x} \right)^{1/2}. \tag{29}$$

The traveltime and the relative geometrical spreading for an elastic VTI model and the acoustic approximations could be computed from selecting the corresponding vertical slowness defined in equations A-2, A-7 and 16. Note that the formula in equation 29 can be applied to both compressional and shear waves.

Numerical examples for the new acoustic approximation

To test the new acoustic approximation, we plot the vertical slowness for the elastic VTI model and the original acoustic and our new acoustic approximations using the model parameters defined in VTI model 1 shown in Figure 8 a, b and c, respectively. One can see that P and S-wave vertical slownesses are shown for the elastic VTI model. For the original acoustic approximation, the P-wave vertical slowness maintains the S-wave artifacts. For our new acoustic approximation, only the P-wave vertical slowness is shown, and the S-wave slowness is totally eliminated. The group velocity could be computed from the corresponding slownesses as shown in equation 22. The plot for the group velocity can be compared with the slowness plot in Figure 5 (b) accordingly. The S-wave artifact in the group velocity plot (Figure 5, b) is caused by the extra slowness shown in Figure 8 (b).

In order to investigate the difference in using the different acoustic approximations, we plot the relative error in the vertical slowness (p_z), the traveltime (t) and the relative geometrical spreading ($\mathcal{L}_N$) in Figure 9, top, middle and bottom, respectively. The error is calculated by measuring the difference with the elastic P-wave solutions for the two defined VTI models. We can see from the plots that for the error in the vertical slowness, our new acoustic approximation is more accurate in the strongly anisotropic model (VTI model 2) while the original acoustic approximation is more accurate in VTI model 1. The error is increasing with

horizontal slowness and is relatively larger in VTI model 2 regardless of the acoustic approximation.

The tendencies of the errors in traveltime and geometrical spreading are very similar. Generally, the error is very small regardless of which acoustic approximation is used. The original acoustic approximation is more accurate in VTI model 1 while less accurate in VTI model 2 for both traveltime and geometrical spreading. For a certain range of the computational offset, our new acoustic approximation is more accurate than the old one and the change in amplitude is smaller. We can tell that our new acoustic approximation achieves generally similar accuracy compared with the original one, and yet, successfully addresses the S-wave artifact issue. This newly proposed acoustic approximation for P-waves can be adopted as an alternative to the original equation for seismic data processing that requires pure P-wave information.

In order to do more accuracy tests, we plot the relative errors in traveltime and relative geometrical spreading versus offset and anellipticity parameter with the old and new acoustic approximations in Figure 10. We can see that generally, the accuracy from the old acoustic approximation is slightly better than our new acoustic counterpart in both traveltime and relative geometrical spreading. However, the errors for both acoustic approximations are neglectably small, and thus, can provide reasonably accurate P-wave approximations.

By using the Dix-type equation (Dix, 1955) to compute the effective model parameters, the new acoustic approximation could be applied for a multi-layered VTI model. We show the relative errors in traveltime and relative geometrical spreading from the old and new acoustic approximations in the multilayered VTI model in Figure 11. The model parameters for the multilayer VTI model are defined in Table 2. We find that similar to the numerical examples in the homogeneous VTI model, the old acoustic approximation is slightly better than our new one while the accuracy is almost the same and the errors are all very small.

Discussions

Our new acoustic approximation is more complicated in comparison with the original equation in the expressions for phase velocity and the corresponding eikonal equation. As opposed to the original eikonal equation shown by Alkhalifah (2000) and shared in equation 23, our new acoustic eikonal equation results in a sixth-order PDE with one real and two complex conjugate solutions, which means solving the new eikonal equation requires an additional computational cost. In order to get rid of the S-wave artifact, we needed to resort to a more complex formula. Different from other attempts in eliminating the S-wave artifact for the acoustic assumption, our acoustic approximation defines the velocities and the kinematics for the pure P-wave in VTI model. The main innovation of this paper is to propose an S-wave-free approximation (S-wave phase velocity is zero for all phase angles) at the expense of increasing the complexity.

We expect that the new equations will be more computationally extensive to apply in modeling and inversion. However, the cleaner wavefields may justify the increase in cost. Considering the rapid advancements in computing, such additional cost may be acceptable. For the eikonal equation, both the 4th and 6th order versions of the acoustic wave equation will require numerical solutions. The difference in cost, in this case, is minor. However, the actual cost difference will depend on the application.

Notice that the wave equation is the central ingredient in describing wave propagation that could be applied in seismic imaging and elastic parameters inversion. Our new acoustic approximation could provide an alternative approach for seismic data processing that requires pure P-wave data at potentially additional cost. We cannot say that our new acoustic approximation is more accurate compared with the standard acoustic approximation in describing P-waves. Most of the cases, their accuracy is almost the same while sometimes our new acoustic approximation is worse. However, what matters is the S-wave-free character

that allows us to use the new equation in applications in which pure P-waves are needed. This often includes applications in waveform inversion and imaging.

The chosen parameters for our accuracy tests meant to represent to strengths of anisotropy. Values associated with real data are even sometimes higher, and our proposed method seems to do well with strong anisotropy.

Our newly proposed acoustic approximation is meant to be an alternative to the original formula (Alkhalifah, 1998) in representing the elastic VTI model for P-waves. The SV shear phase velocity is set to zero for all phase angles while for standard acoustic approximation (Alkhalifah, 1998) only vertical S velocity is zero. Compared with the original equation (Alkhalifah, 1998), the expression becomes more complicated while it may not improve the accuracy of P-wave description. However, it provides a S-wave free wavefield necessary for many applications.

Conclusion

We propose a new acoustic approximation for P-waves in elastic VTI models free of the S-wave artifact. Instead of setting the vertical S-wave velocity to zero, we derive an angle-dependent vertical S-wave phase velocity that guarantees a zero-value shear wave velocity at all directions. To describe the kinematics of the new acoustic approximation, the P-wave vertical slowness is derived. It can be used for imaging applications. The corresponding eikonal equation for the new acoustic approximation is a sixth-order nonlinear PDE, which can be used to describe the pure P traveltimes. The corresponding perturbation-based approximation for the new eikonal equation is used to compare the accuracy of this new approximation as compared with the original formula. The new approximation yields accurate traveltimes free of shear wave artifacts, but potentially at an additional cost considering the higher-order nature of the formula.

Acknowledgments

We would like to acknowledge the Kyoto University, the Norwegian University of Science and Technology and King Abdullah University of Science and Technology for the support. We also thank the Editor Dr. J. Shragge, Associate Editor Dr S. Hestholm, and Reviewers Dr. I. Ravve, Dr. P. Golikov, Dr U. Waheed and three anonymous reviewers for their comments and helpful suggestions.

Appendix A. The vertical slowness for P and S-waves in elastic VTI model

The characteristic Christoffel equation in VTI media is defined by setting the determinant of the matrix N that is represented by six independent density normalized stiffness coefficients c_{ij} to be zero ($\det \mathbf{N} = 0$),

$$\mathbf{N} = \begin{pmatrix} C_{11}p_x^2 + C_{44}p_z^2 - 1 & 0 & (C_{13} + C_{44})p_x p_z \\ 0 & C_{66}p_x^2 + C_{44}p_z^2 - 1 & 0 \\ (C_{13} + C_{44})p_x p_z & 0 & C_{44}p_x^2 + C_{33}p_z^2 - 1 \end{pmatrix}, \tag{A-1}$$

The corresponding P and S-wave vertical slownesses are computed by solving the cubic equation ($\det \mathbf{N} = 0$) given by

$$\begin{aligned} p_{z,P} &= \sqrt{\frac{C_{33} + C_{44} + \left(C_{13}^2 - C_{11}C_{33} + 2C_{13}C_{44}\right)p_x^2 - K}{2C_{33}C_{44}}}, \\ p_{z,S} &= \sqrt{\frac{C_{33} + C_{44} + \left(C_{13}^2 - C_{11}C_{33} + 2C_{13}C_{44}\right)p_x^2 + K}{2C_{33}C_{44}}}, \end{aligned} \tag{A-2}$$

where

$$K = \sqrt{\left(C_{33} + C_{44} + \left(C_{13}^2 - C_{11}C_{33} + 2C_{13}C_{44}\right)p_x^2\right)^2 - 4C_{33}C_{44}\left(C_{11}p_x^2 - 1\right)\left(C_{44}p_x^2 - 1\right)}. \tag{A-3}$$

These stiffness coefficients could be expressed using the anisotropy parameters

$$\begin{aligned} C_{11} &= (1 + 2\varepsilon)V_{P0}^2, \\ C_{33} &= V_{P0}^2, \\ C_{44} &= V_{S0}^2, \\ C_{13} &= \sqrt{(V_{P0}^2 - V_{S0}^2)((1 + 2\delta)V_{P0}^2 - V_{S0}^2)} - V_{S0}^2. \end{aligned} \tag{A-4}$$

The elastic P and S-waves vertical slownesses are given by the anisotropy parameters

$$\begin{aligned} p_{z,p}^2 &= \frac{1}{2}\frac{V_{s0}^2\left(1 - p_x^2V_{p0}^2\right) - V_{p0}^2\left[p_x^2\left(2\eta V_{pn}^2 + V_{s0}^2\right) - 1\right] - \sqrt{K}}{V_{p0}^2V_{s0}^2}, \\ p_{z,s}^2 &= \frac{1}{2}\frac{V_{s0}^2\left(1 - p_x^2V_{p0}^2\right) - V_{p0}^2\left[p_x^2\left(2\eta V_{pn}^2 + V_{s0}^2\right) - 1\right] + \sqrt{K}}{V_{p0}^2V_{s0}^2}, \end{aligned} \tag{A-5}$$

with

$$\begin{aligned} K = &-4V_{p0}^2V_{s0}^2\left[(1 + 2\eta)p_x^2V_{pn}^2 - 1\right]\left(p_x^2V_{s0}^2 - 1\right) \\ &+ \left\{V_{s0}^2\left(p_x^2V_{pn}^2 - 1\right) + V_{p0}^2\left[p_x^2\left(2\eta V_{pn}^2 + V_{s0}^2\right)\right]\right\}^2. \end{aligned} \tag{A-6}$$

The vertical slowness for the acoustic P-wave is obtained by adopting the acoustic assumption (value of the vertical S-wave velocity is zero) given by (Alkhalifah, 1998)

$$p_{z,p}^2 = \frac{V_{pn}^2 p_x^2 (1+2\eta) - 1}{V_{p0}^2 \left[V_{pn}^2 p_x^2 (1+2\eta) - 1 \right] - V_{p0}^2 p_x^2 V_{pn}^2}. \quad \text{(A-7)}$$

Notice that the exact solution for P-wave velocity is quadratic while our new acoustic form solution is cubic. The reason for the increase in complexity is that by substituting the vertical S-wave velocity back to compute the P-wave solution that is free of S-waves, the vertical S-wave velocity becomes a function of phase angle instead of a set parameter.

Appendix B. The solution for the cubic equation

The phase velocity in the VTI model satisfies the following eikonal form:

$$\begin{aligned} v_p^2(\theta) &= \frac{1}{p_x^2 + p_z^2}, \\ \theta &= \arctan\frac{p_x}{p_z}, \end{aligned} \tag{B-1}$$

where p_x and p_z are the projections of the horizontal and vertical slowness vectors with $p_x = \sin(\theta)/v(\theta)$ and $p_z = \cos(\theta)/v(\theta)$. In order to compute the vertical slowness for the new acoustic P-wave, by substituting equation B-1 into equation 11 and replacing the phase angle with θ in equation B-1, we obtain a cubic equation given by

$$p_z^6 + Bp_z^4 + Cp_z^2 + D = 0, \tag{B-2}$$

where the functions B, C and D are given by the model parameters

$$\begin{aligned} B &= \frac{p_x^2\left(v_{p0}^2 + 2v_{pn}^2\right) - 1}{v_{p0}^2}, \\ C &= \frac{p_x^2\left(\left(2(1+\eta)\,p_x^2 v_{pn}^2 - 1\right)\left(v_{p0}^2 + v_{pn}^2\right)\right)}{v_{p0}^4}, \\ D &= \frac{p_x^4 v_{pn}^2\left(1+2\eta\right)\left(\left(1+2\eta\right)p_x^2 v_{pn}^2 - 1\right)}{v_{p0}^4}. \end{aligned} \tag{B-3}$$

There are different ways to solve this cubic equation (equation B-2) for the corresponding solutions. The discriminant of the cubic equation is used to determine the number of real and complex roots given by

$$\Delta = 18BCD - 4B^3D + B^2C^2 - 4C^3 - 27D^2. \tag{B-4}$$

If $\Delta > 0$, the cubic equation shown in equation B-2 has three distinct real roots (Tsvankin, 1997; Xu and Stovas, 2019) given by

$$p_z^2 = 2\sqrt{-\frac{P}{3}}\cos\left[\frac{1}{3}\cos^{-1}\left(\frac{3Q}{2P}\sqrt{-\frac{3}{P}}\right) - \frac{2N\pi}{3}\right] - \frac{B}{3}. \tag{B-5}$$

Parameters P and Q are given by

$$P = \frac{3C - B^2}{3},$$
$$Q = \frac{2B^3 - 9BC + 27D}{27}. \tag{B-6}$$

$N = 0,1,2$ corresponds to three different real solutions.

When the discriminant is negative ($\Delta < 0$), then the cubic equation has one real root and two complex conjugate roots.

In our VTI model, only one real solution exists. The real solution is given by

$$p_z^2 = \frac{1}{6}\left[-2B + \frac{2 \times 2^{1/3} f_1}{\left(f_2 + f_3 \right)^{1/3}} + 2^{2/3} \left(f_2 + f_3 \right)^{1/3} \right], \tag{B-7}$$

The two complex conjugate roots are given by

$$p_{z,1}^2 = \frac{1}{12}\left[-4B - \frac{2i \times 2^{1/3} (\sqrt{3} - i) f_1}{\left(f_2 + f_3 \right)^{1/3}} - 2^{2/3} (1 - i\sqrt{3}) \left(f_2 + f_3 \right)^{1/3} \right],$$
$$p_{z,2}^2 = \frac{1}{12}\left[-4B - \frac{2i \times 2^{1/3} (\sqrt{3} + i) f_1}{\left(f_2 + f_3 \right)^{1/3}} - 2^{2/3} (1 + i\sqrt{3}) \left(f_2 + f_3 \right)^{1/3} \right], \tag{B-8}$$

with

$$f_1 = B^2 - 3C,$$
$$f_2 = -2B^3 + 9BC - 27D, \tag{B-9}$$
$$f_3 = 3\sqrt{3}\sqrt{-B^2C^2 + 4C^3 + 4B^3D - 18BCD + 27D^2}.$$

References

Alkhalifah, T., 1998, Acoustic approximations for processing in transversely isotropic media: Geophysics, **63**, 623–631.

Alkhalifah, T., 2000, An acoustic wave equation for anisotropic media: Geophysics, **65**, 1239–1250.

Alkhalifah, T., 2011, Scanning anisotropy parameters in complex media: Geophysics, **76**, no. 2, U13–U22.

Alkhalifah, T., 2013, Residual extrapolation operators for efficient wavefield construction: Geophysical journal international, **193**, 1027-1034.

Alkhalifah, T., and R, É, Plessix, 2014, A recipe for practical full-waveform inversion in anisotropic media: An analytical parameter resolution study: Geophysics, **79**, no. 3, R91–R101.

Alkhalifah, T., and S. Fomel, 2011, The basic components of residual migration in VTI media using anisotropy continuation: Journal of Petroleum Exploration and Production Technology: **1**, 17–22.

Alkhalifah, T., and Tsvankin, I., 1995, Velocity analysis for transversely isotropic media: Geophysics, **60**, 1550–1566.

Berryman, J., 1979, Long-wave elastic anisotropy in transversely isotropic media: Geophysics, **44**, 896-917.

Cheng, J., and W. Kang, 2014, Simulating propagation of separated wave modes in general anisotropic media, Part I: qP-wave propagators: Geophysics, **79**, no. 1, C1-C18.

Cohen, J. K., and Bleistein, N., 1979, Velocity inversion procedure for acoustic waves: Geophysics, **44**, 1077–1087.

Cohen, J., 1996, Analytic study of the effective parameters for determination of the NMO velocity function in transversely isotropic media: Center for Wave Phenomena, Colorado School of Mines (CWP-191).

Dellinger, J., and Muir, F., 1988, Imaging reflections in elliptically anisotropic media: Geophysics, **53**, 1616–1618.

Dix, C. H., 1955, Seismic velocities from surface measurements: Geophysics, **20**, 68–86.

Du, X., R. P. Fletcher, and P. J. Fowler, 2010, Pure p-wave propagators versus pseudo-acoustic propagators for RTM in VTI media: 72nd Annual International Conference and Exhibition, EAGE, Extended Abstracts, 382–386.

Finkelstein, B., and R. Kastner, 2007, Finite difference time domain dispersion reduction schemes: Journal of Computational Physics, **221**, 422–438.

Fletcher, R. P., X. Du, and P. J. Fowler, 2009, Reverse time migration in tilted transversely isotropic (TTI) media: Geophysics, **74**, no, 6, WCA179–WCA187.

Fomel, S., L. Ying, and X. Song, 2013, Seismic wave extrapolation using lowrank symbol approximation: Geophysical Prospecting, **61**, 526–536.

Gholami, Y., R. Brossier, S. Operto, A. Ribodetti, and J. Virieux, 2013, Which parameterization is suitable for acoustic vertical transverse isotropic full waveform inversion? Part 1: Sensitivity and trade-off analysis: Geophysics, **78**, no. 2, R81–R105.

Grechka, V., L. Zhang, and R. James,. Rector, 2004, Shear waves in acoustic anisotropic media: Geophysics, **69**, 576–582.

Ibanez-Jacome, W., T. Alkhalifah , and U. Bin Waheed, 2013, Effective Orthorhombic Anisotropic Models for Wavefield Extrapolation: Geophysical Journal International, **198**, 1653-1661.

Jin, S., and A. Stovas, 2018, S-wave kinematics in acoustic transversely isotropic media with a vertical symmetry axis: Geophysical Prospecting, **66**, 1123–1137.

Li, V., H. Wang, I. Tsvankin, E. Diaz, and T. Alkhalifah, 2017, Inversion gradients for acoustic VTI wavefield tomography: Geophysics, **82**, no. 4, WA55–WA65.

Li, V., I. Tsvankin, and T. Alkhalifah, 2016, Analysis of RTM extended images for VTI media: Geophysics, **81**, no. 3, S139-S150.

Liu, Y., and M. K. Sen, 2010, Acoustic VTI modeling with a time-space domain dispersion-relation-based finite-difference scheme: Geophysics, **75**, no. 3, A11-A17.

Pestana, R., and P. L. Stoffa, 2010, Time evolution of the wave equation using rapid expansion method: Geophysics, **75**, no. 4, T121–T131.

Song, X., and S. Fomel, 2011, Fourier finite-difference wave propagation: Geophysics, **76**, no. 5, T123-T129.

Song, X., and T. Alkhalifah, 2013, Modeling of pseudoacoustic P-waves in orthorhombic media with a low-rank approximation: Geophysics, **78**, no. 4, C33-C40.

Thomsen, L., 1986, Weak elastic anisotropy: Geophysics, **51**, 1954– 1966.

Tsvankin, I., 2012, Seismic signatures and analysis of reflection data in anisotropic media: Society of Exploration Geophysicists, third edition.

Waheed, U., and T. Alkhalifah, 2015, An efficient wave extrapolation method for anisotropic media with tilt: Geophysical prospecting, **63**, 1126–1141.

Wang, X., and I. Tsvankin, 2009, Estimation of interval anisotropy parameters using velocity-independent layer stripping: Geophysics, **74**, no. 5, WB117-WB127.

Xu, S., A. Stovas and Q. Hao, 2017, Perturbation-based moveout approximations in anisotropic media: Geophysical Prospecting, **65**, 1218-1230.

Xu, S., and A. Stovas, 2017, A new parameterization for acoustic orthorhombic media: Geophysics, **82**, no. 6, C229-C240.

Xu, S., and A. Stovas, 2018, Triplications on traveltime surface for pure and converted wave modes in elastic orthorhombic media: Geophysical Journal International, **215**, 677-694.

Xu, S., and A. Stovas, 2019, Singularity point in effective orthorhombic medium computed from zero- and infinite-frequency limit: Geophysical Journal International, **217**, 319-330.

Xu, S., T. Alkhalifah, and A. Stovas, 2016, Estimation of the anisotropy parameters from imaging moveout of diving wave in a factorized VTI medium: Geophysics, **81**, no.4, C139-C150.

Zhou, H., G. Zhang. and R. Bloor, 2006, An anisotropic acoustic wave equation for VTI media: 68th EAGE meeting, Vienna, Austria, Extended Abstracts.

Figure captions

Figure 1. The phase (top) and group (bottom) velocities for the elastic P- and S-waves computed for two defined VTI models. The model parameters are defined in Table 1. The curve for the P-wave in VTI models 1 and 2; and S-waves in VTI models 1 and 2 are shown in solid blue, dashed blue, solid red and dashed red lines, respectively.

Figure 2. The relative errors in the P-wave phase (left) and group (right) velocities using the standard acoustic assumption for the two defined VTI models. The model parameters are defined in Table 1. The errors in the computation in VTI model 1 and 2 are shown in blue and red lines, respectively.

Figure 3. A snapshot in time of the wavefield from the original acoustic wave equation. The S-wave artifact could be seen in the plot.

Figure 4. The polar plot for the vertical S-wave function in the phase domain used for our new acoustic assumption computed for the two defined VTI models.

Figure 5. The group velocity computed for VTI model 1 for the elastic VTI case (a), the original acoustic approximation (b) and our new acoustic approximation (c), top, middle and bottom, respectively. The P and S-wave velocities are shown in blue and red lines, respectively. Note that the expression for the S-wave artifact could be found in Song and Stovas (2018).

Figure 6. The relative error from using the two acoustic approximations for the two VTI models for both phase (top) and group (bottom) velocities. The relative error for the standard acoustic assumption in VTI models 1 and 2 and our new acoustic approximation in VTI models 1 and 2 are shown in solid red, dashed red, solid blue and dashed blue lines, respectively.

Figure 7. The discriminant of the cubic equation computed from the solution of the slowness in our new acoustic approximation versus two anisotropic parameters δ and ε. The model parameters for this stability analysis are: $v_{p0} = 3km/s$, $v_{s0} = 1km/s$ and $z_0 = 1km$.

Figure 8. The vertical slowness for the elastic VTI case (top), the standard acoustic VTI approximation (middle) and our pure acoustic VTI approximation (bottom) using the model parameters defined in VTI model 1.

Figure 9. The relative errors in the vertical slowness (top) and the corresponding traveltime (middle) and the relative geometrical spreading (bottom) using two acoustic assumptions computed for the two introduced VTI models. The relative error for the standard acoustic assumption in VTI models 1 and 2 and our new acoustic assumption in VTI models 1 and 2 are shown in solid red, dashed red, solid blue and dashed blue lines, respectively.

Figure 10. The relative errors in traveltime and relative geometrical spreading versus offset and anellipticity parameter from the old and new acoustic approximations. The model parameters are: $v_{p0} = 3km/s$, $v_{pn} = 4km/s$, $v_{s0} = 1km/s$ and $z_0 = 1km$.

Figure 11. The relative errors in traveltime and relative geometrical spreading from the old and new acoustic approximations in the multilayered VTI model. The model parameters are defined in Table 2.

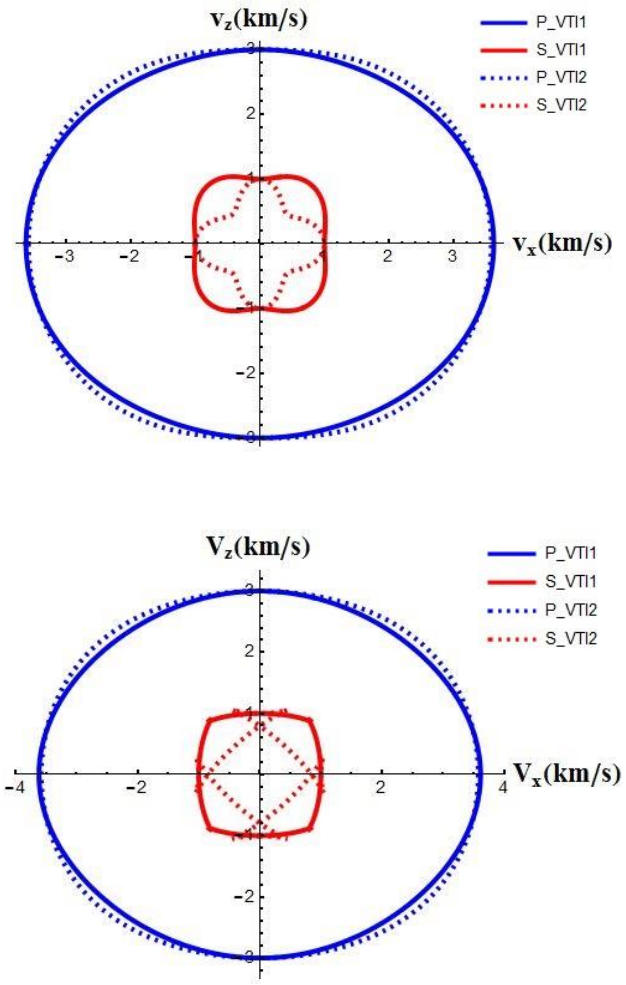

Figure 1. The phase (top) and group (bottom) velocities for the elastic P- and S-waves computed for two defined VTI models. The model parameters are defined in Table 1. The curve for the P-wave in VTI models 1 and 2; and S-waves in VTI models 1 and 2 are shown in solid blue, dashed blue, solid red and dashed red lines, respectively.

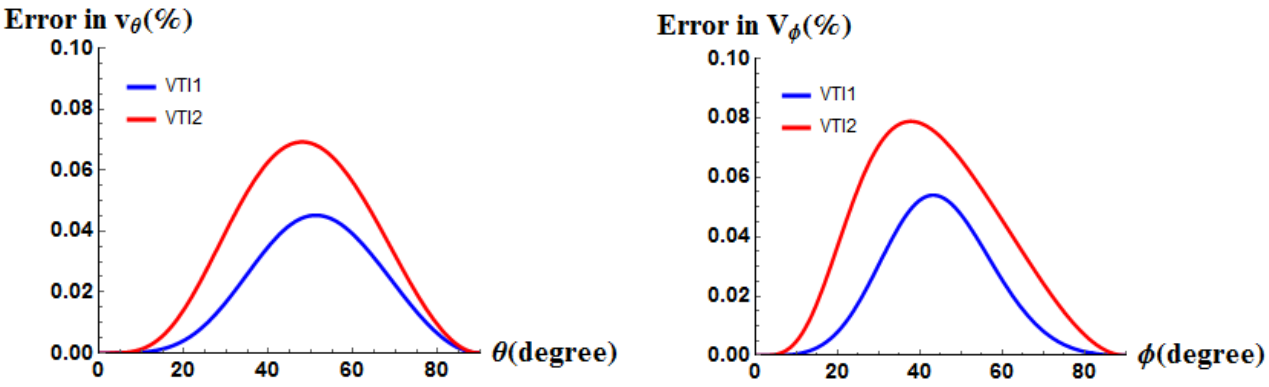

Figure 2. The relative errors in the P-wave phase (left) and group (right) velocities using the standard acoustic assumption for the two defined VTI models. The model parameters are defined in Table 1. The errors in the computation in VTI model 1 and 2 are shown in blue and red lines, respectively.

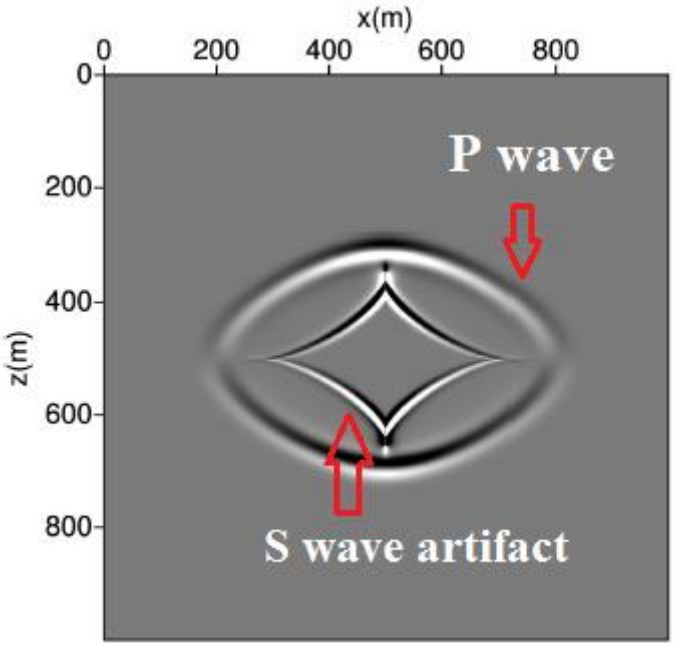

Figure 3. A snapshot in time of the wavefield from the original acoustic wave equation. The S-wave artifact could be seen in the plot.

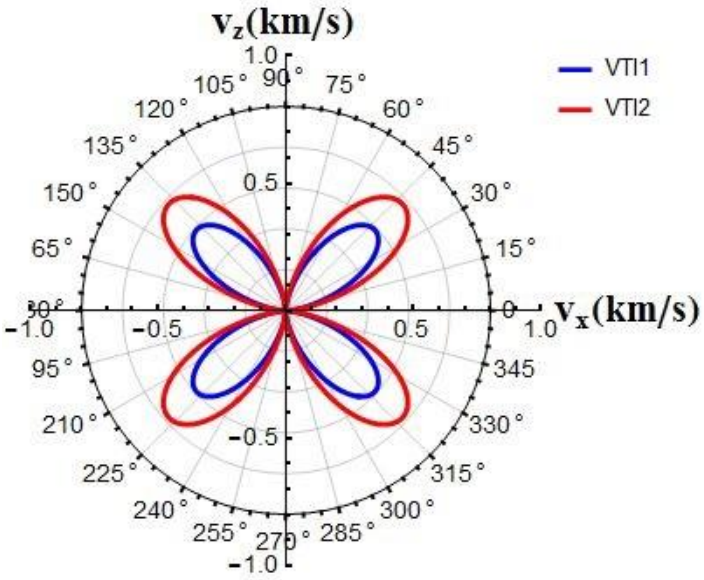

Figure 4. The polar plot for the vertical S-wave function in the phase domain used for our new acoustic assumption computed for the two defined VTI models.

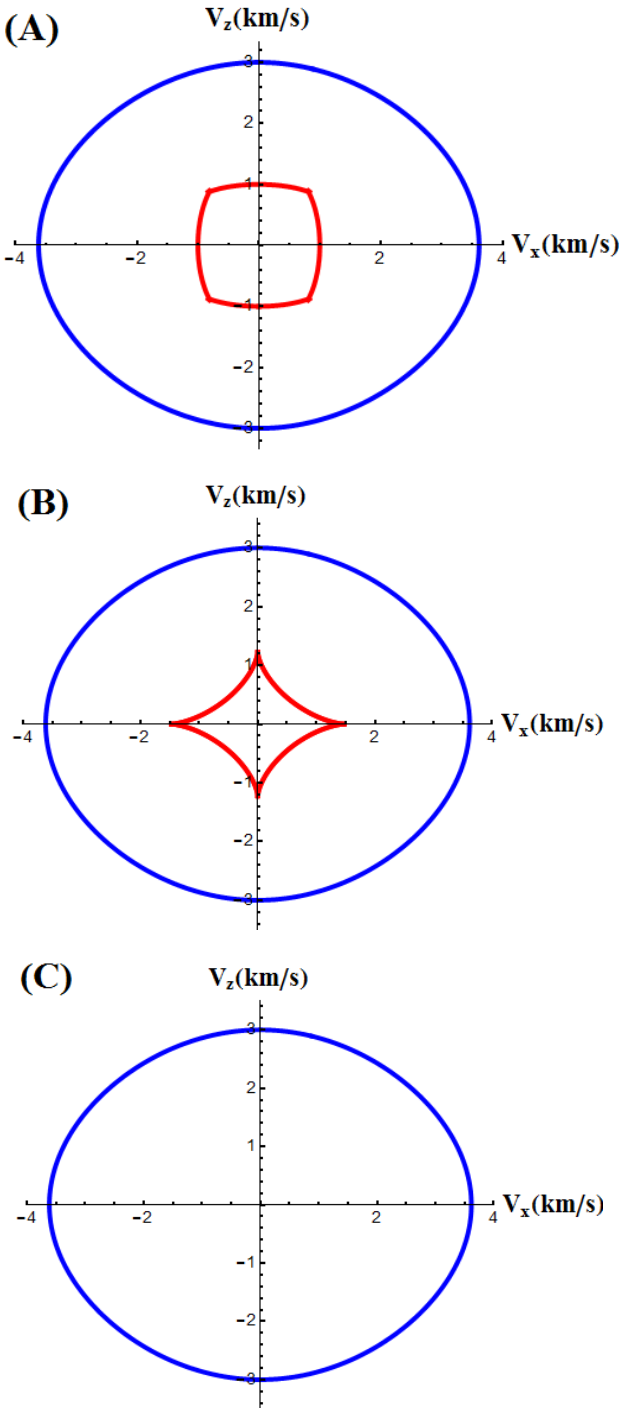

Figure 5. The group velocity computed for VTI model 1 for the elastic VTI case (a), the original acoustic approximation (b) and our new acoustic approximation (c), top, middle and bottom, respectively. The P and S-wave velocities are shown in blue and red lines, respectively. Note that the expression for the S-wave artifact could be found in Song and Stovas (2018).

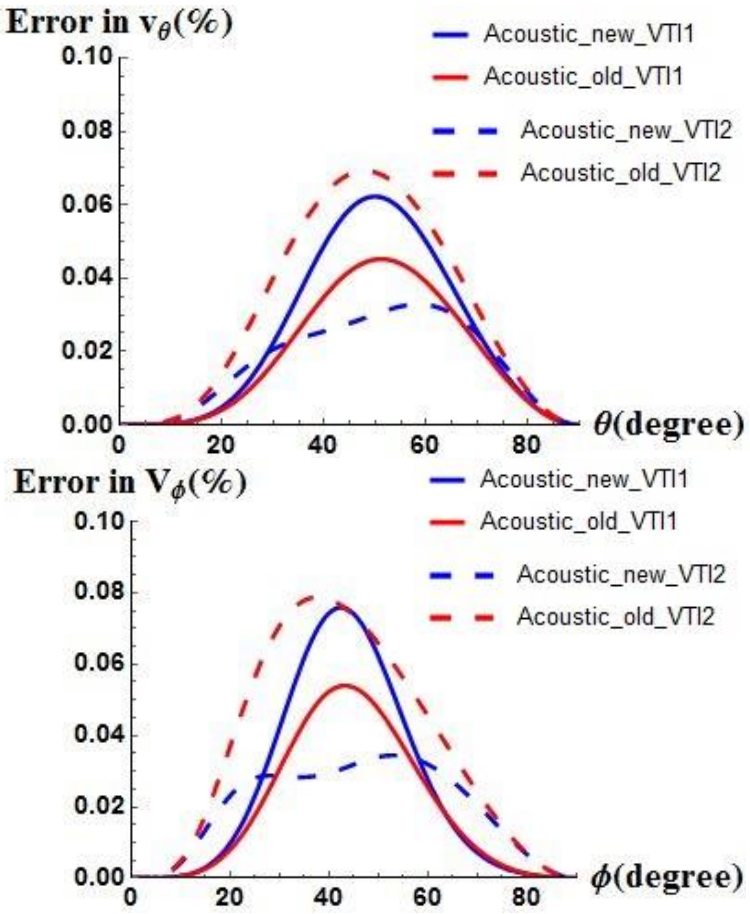

Figure 6. The relative error from using the two acoustic approximations for the two VTI models for both phase (top) and group (bottom) velocities. The relative error for the standard acoustic assumption in VTI models 1 and 2 and our new acoustic approximation in VTI models 1 and 2 are shown in solid red, dashed red, solid blue and dashed blue lines, respectively.

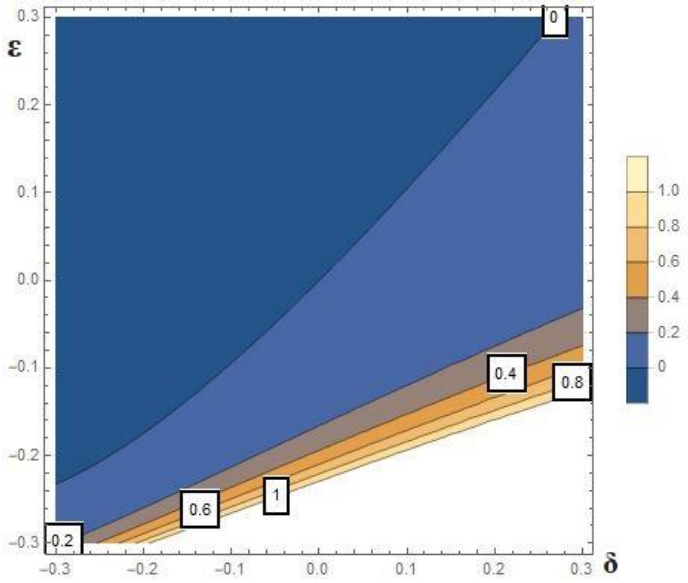

Figure 7. The discriminant of the cubic equation computed from the solution of the slowness in our new acoustic approximation versus two anisotropic parameters δ and ε. The model parameters for this stability analysis are: $v_{p0} = 3km/s$, $v_{s0} = 1km/s$ and $z_0 = 1km$.

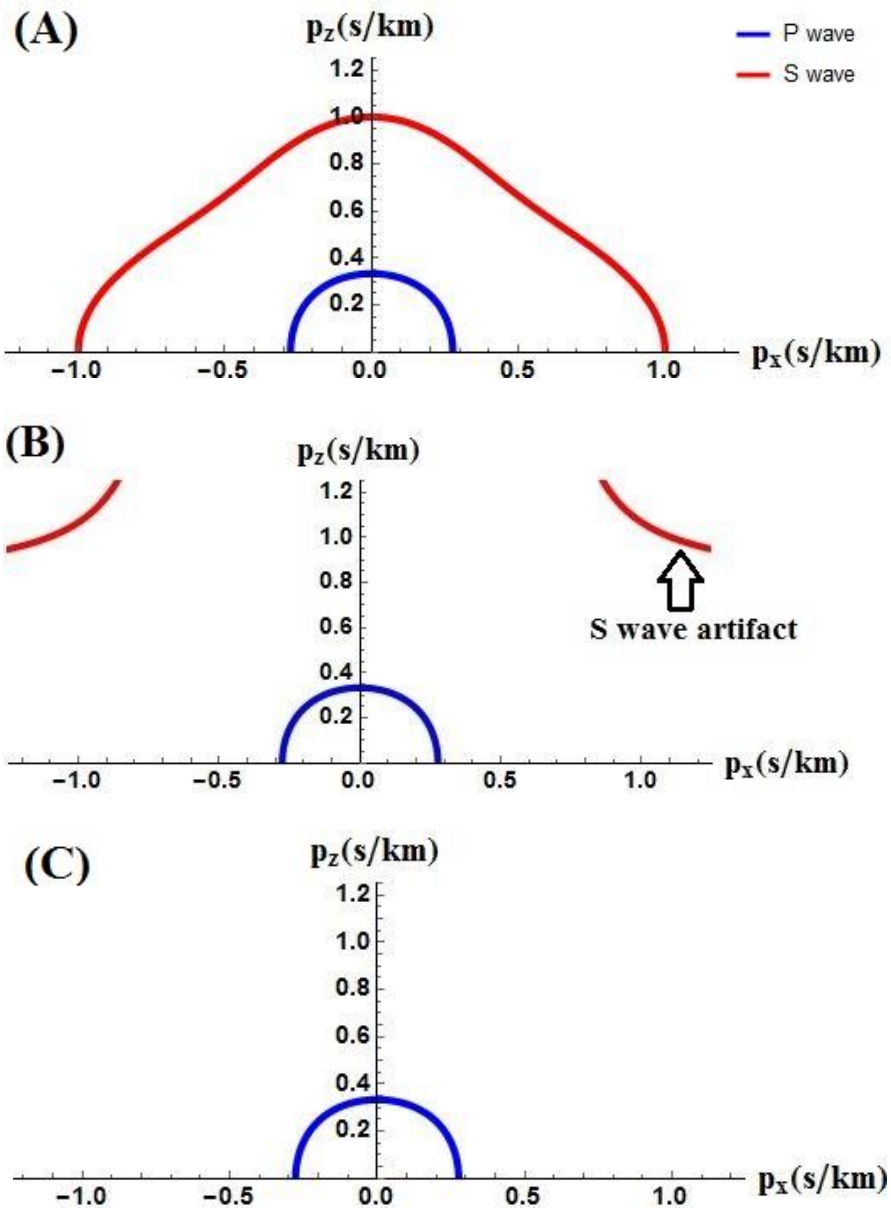

Figure 8. The vertical slowness for the elastic VTI case (top), the standard acoustic VTI approximation (middle) and our pure acoustic VTI approximation (bottom) using the model parameters defined in VTI model 1.

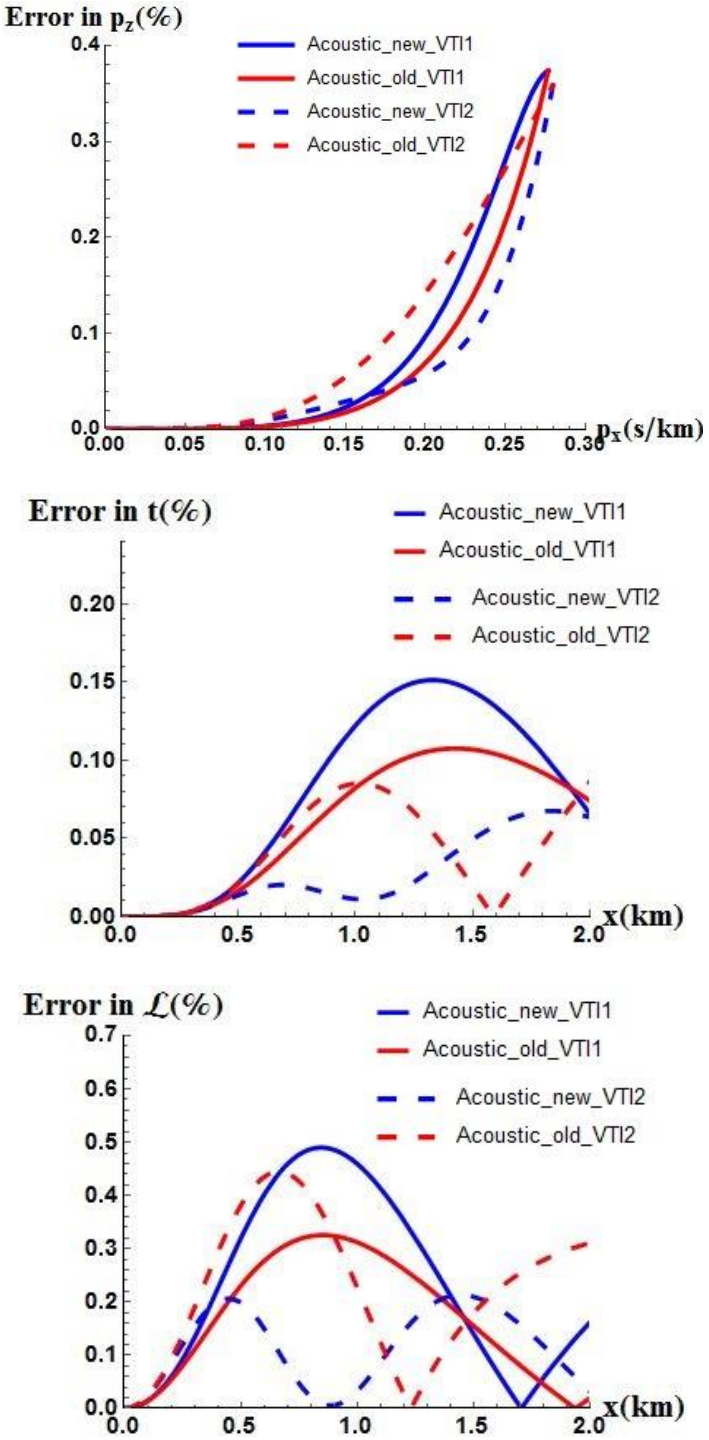

Figure 9. The relative errors in the vertical slowness (top) and the corresponding traveltime (middle) and the relative geometrical spreading (bottom) using two acoustic assumptions computed for the two introduced VTI models. The relative error for the standard acoustic assumption in VTI models 1 and 2 and our new acoustic assumption in VTI models 1 and 2 are shown in solid red, dashed red, solid blue and dashed blue lines, respectively.

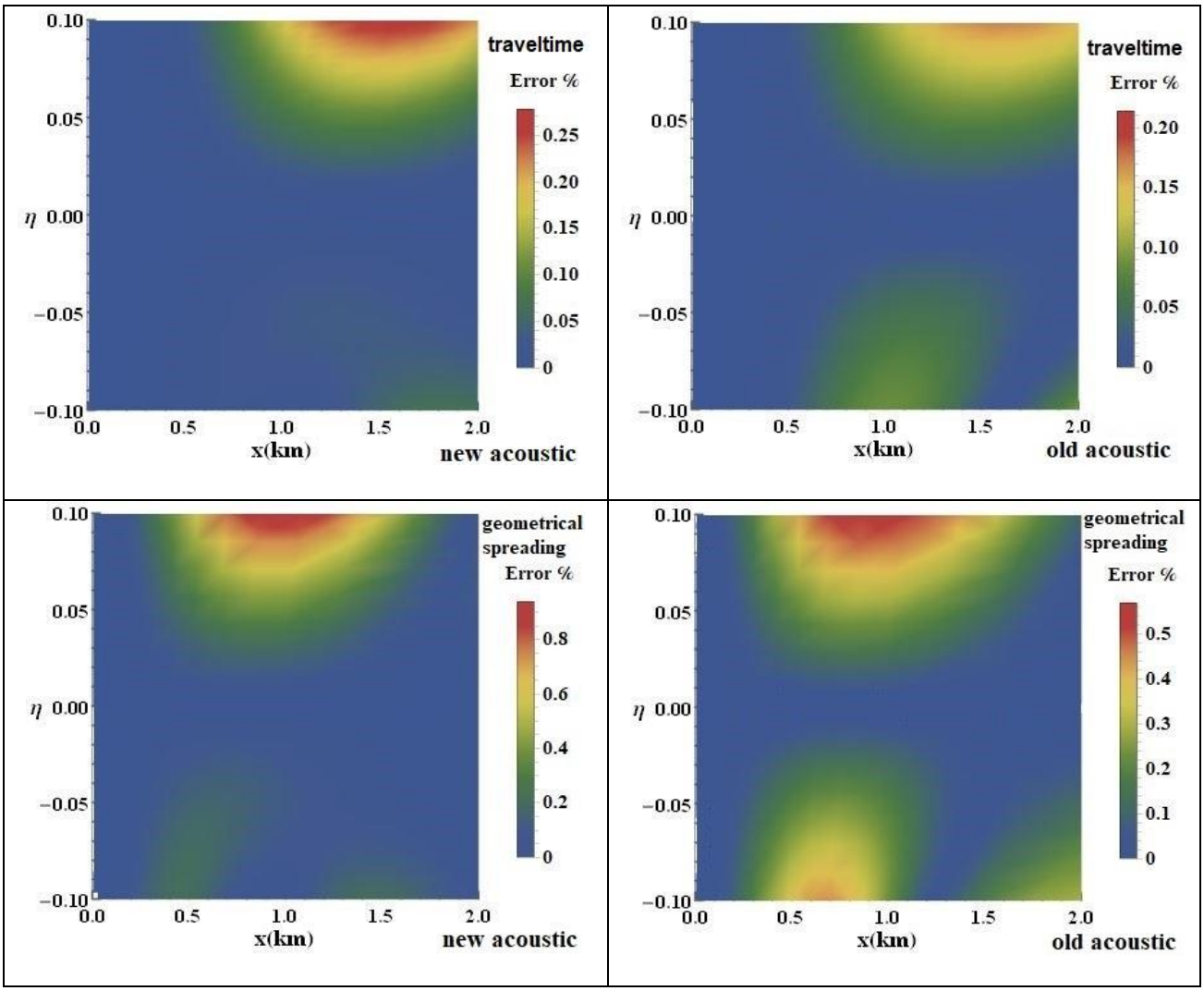

Figure 10. The relative errors in traveltime and relative geometrical spreading versus offset and anellipticity parameter from the old and new acoustic approximations. The model parameters are: $v_{p0} = 3km/s$, $v_{pn} = 4km/s$, $v_{s0} = 1km/s$ and $z_0 = 1km$.

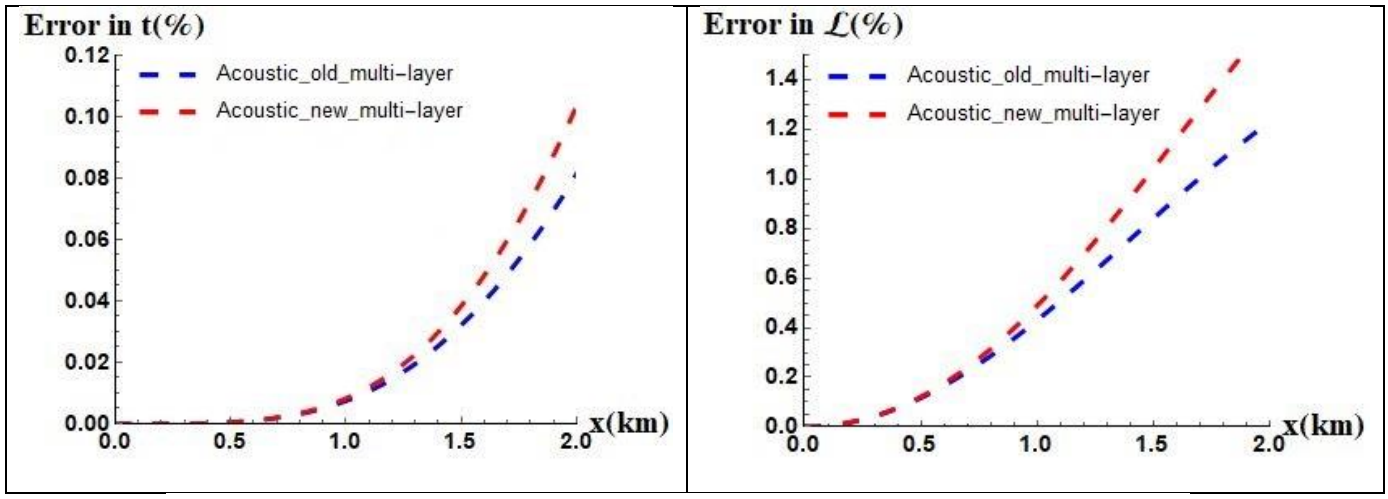

Figure 11. The relative errors in traveltime and relative geometrical spreading from the old and new acoustic approximations in the multilayered VTI model. The model parameters are defined in Table 2.

Table caption

Table 1. The model parameters for two VTI models.

Table 2. The model parameters for the multilayered VTI model.

	$v_{p0}(km/s)$	$v_{s0}(km/s)$	$v_{pn}(km/s)$	η
Model 1	3	1	3.3	0.1
Model 2	3	1	4	-0.1

Table 1. The model parameters for two homogeneous VTI models.

	$v_{p0}(km/s)$	$v_{s0}(km/s)$	$v_{pn}(km/s)$	η	$z_0(km)$
Layer 1	1.5	1	1.7	0.1	0.3
Layer 2	1.8	1	2	0.12	0.7
Layer 3	2	1	2.3	0.18	1
Layer 4	2.2	1	2.5	0.2	1.5
Layer 5	2.5	1	2.8	0.22	0.5

Table 2. The model parameters for the multilayered VTI model.